

Supporting quantum technologies with a micron-scale silicon photonics platform

Matteo Cherchi*, Arijit Bera, Antti Kemppinen, Jaani Nissilä, Kirsi Tappura, Marco Caputo, Lauri Lehtimäki, Janne Lehtinen, Joonas Govenius, Mika Prunnila, and Timo Aalto
VTT – Technical Research Centre of Finland Ltd, Tietotie 3, 02150 Espoo, Finland

ABSTRACT

VTT micron-scale silicon photonics platform can play a significant role in the second quantum revolution, supporting not only quantum photonics but also solid-state quantum systems. Quantum photonics can benefit from the unique properties of the platform, a distinctive example application being quantum key distribution, where we are developing receivers to support its large-scale deployment. On the other hand, we are using our photonic integration technology also to aid scaling-up superconducting quantum computers, by controlling and reading the qubits in the cryostat through classical optical links. I will cover all these developments showing our recent results, ongoing activities, and future plans.

Keywords: silicon photonics, quantum key distribution, quantum computers, cryogenic photonics, superconducting nanowire single photon detectors, quantum technologies

1. INTRODUCTION

We are presently living the so-called second quantum revolution, where the focus has shifted from pure science to technologies and applications. Photonic technologies are expected to play a major role, not only through quantum light, but also resorting to classical light to aid solid-state quantum systems. In particular, photonic integrated circuits offer unique opportunities for different quantum technologies, to scale up system complexity and integration density, while providing unmatched performance and stability. In this regard, VTT micron-scale silicon photonics platform¹ can weigh in with a unique set of properties and building blocks. This includes low propagation losses (down to 4 dB/m demonstrated to date²), broadband and low-loss coupling to fibres (≈ 0.5 dB), fast (> 40 GHz) and responsive (≈ 1 A/W) integrated germanium photodetectors³, up-reflecting mirrors for broadband and low-loss coupling to arrays of single photon detectors, tight bends⁴ enabling high integration density, efficient phase shifters, low-loss Mach-Zehnder interferometers, multi-million Q ring resonators⁵, polarization insensitive operation, polarization splitters⁶ and rotators, including all-silicon Faraday rotators⁷. A relevant example application is large-scale deployment of quantum key distribution (QKD), for which we are developing efficient multiplexed receivers. A second interesting case is the use of our photonic integration technology to scale-up superconducting quantum computers, by controlling and reading out the qubits in the cryostat through classical optical links. In this case the major challenge is developing suitable electrical-to-optical and optical-to-electrical converters operating at cryogenic temperatures. In the following, we will cover these ongoing developments showing our recent results as well as our plans to exploit the platform in other promising quantum applications. In §2, we will first give an overview of the thick silicon photonics platform, with a special focus on the most relevant features for quantum applications. In sections 3 and 4, we will cover the ongoing developments for QKD and quantum computers, and then conclude in §5 briefly mentioning other promising future applications, together with some conclusions.

2. OVERVIEW OF VTT THICK SOI PLATFORM

We can divide the building blocks of the platform into two main categories: passives and actives. In this context, with “active” we mean anything requiring an electrical control, like a thermo-optic phase shifter or an electro-optic modulator, or electrical readout, like a photodiode. A summary of the building blocks available on the platform is sketched in Figure 1. A basic building block is actually missing from the picture, that is the PIN phase modulator based on plasma dispersion, which has a structure somewhat similar to that of the implanted heater, but with an additional N-type implantation on the opposite side of the P-type implantation (see §2.2). We fabricate our photonic integrated circuits (PICs) on 150 mm SOI wafers (to be soon upgraded to 200 mm) with 3 μm thick device layer (± 100 nm uniformity), using a UV stepper (365 nm wavelength) and a modified Bosch process^{8,9} to etch the silicon waveguides.

*matteo.cherchi@vtt.fi; phone +358 40 684 9040, ORCID [0000-0002-6233-4466](https://orcid.org/0000-0002-6233-4466), www.vtt.fi

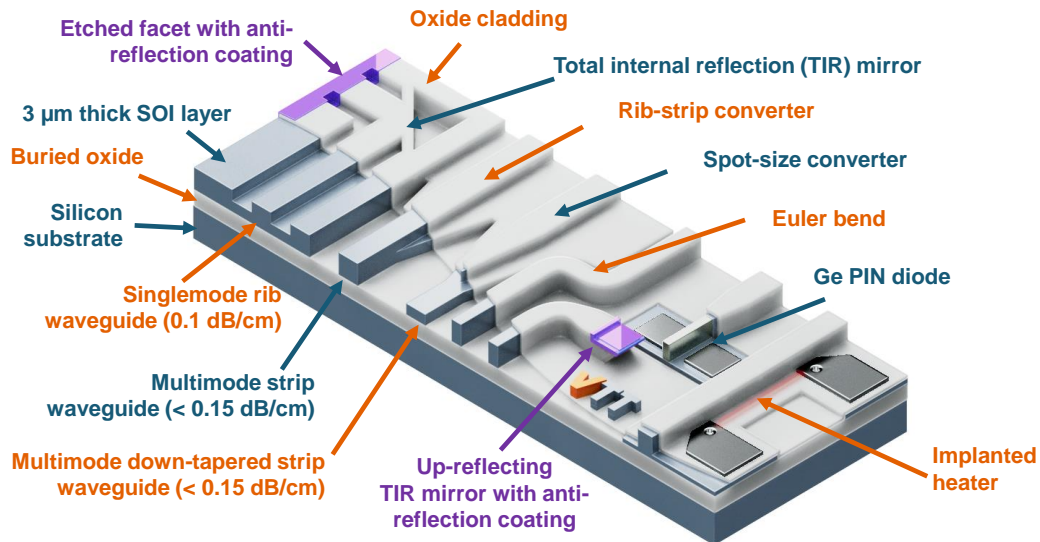


Figure 1. Sketch of the main building blocks available on the thick-SOI platform. Typical thickness of the device layer is $3\ \mu\text{m}$, whereas the buried oxide (BOX) thickness can vary from $400\ \text{nm}$ to $3\ \mu\text{m}$. We call “active” all building blocks requiring electrical pads for either control or readout.

2.1 Passive building blocks

Types of waveguides

The four main waveguide types available on the platform are: the rib waveguide, where two trenches are partially etched (typically $1.2\ \mu\text{m}$ deep etch) on the two sides of the waveguide. Singlemode operation can be achieved for both TE and TM polarisation with a suitable choice of the rib width (typically $\leq 3\ \mu\text{m}$). On the contrary, all four possible strip waveguide cross sections (through etched strip, through etched down-tapered strip, and versions of both with a thin unetched silicon pedestal) are inherently multimode. Nevertheless, we carefully design the optical circuits to ensure that excitation of the higher order modes (HOMs) is always negligible in the connecting waveguides, ensuring effective singlemode operation.

I/O coupling

We fabricate the vertical waveguide facets of our PICs at wafer scale, by first etching the silicon facet and then depositing a suitable anti-reflection coating, which can be made of either a single dielectric layer or multiple layers.

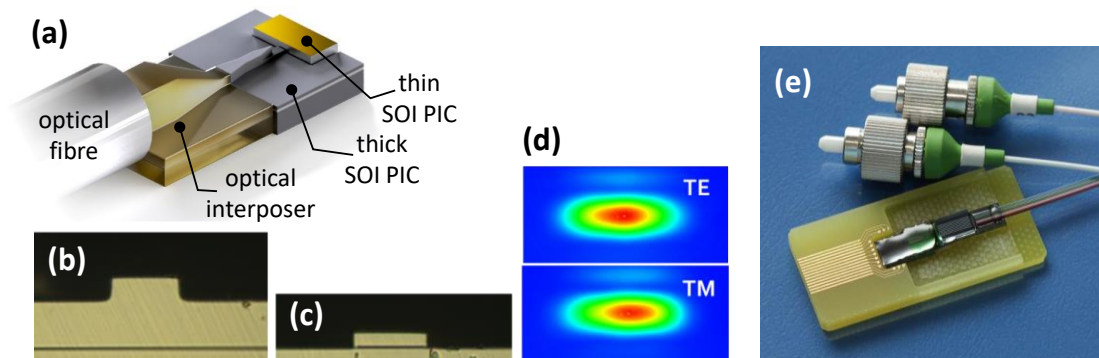


Figure 2. (a) Sketch of different mode size conversion starting from a SMF coupled to the $3\ \mu\text{m}$ thick waveguides of a thick SOI PIC using an optical interposer fabricated on $12\ \mu\text{m}$ thick SOI. The sketch shows also how the mode size can be reduced further even to match submicron waveguides on a flip-chip bonded PIC that can be evanescently coupled through suitable inverse tapers; (b) micrograph of $12\ \mu\text{m}$ thick rib waveguide of a fabricated optical interposer and (c) micrograph of a strip waveguide polished down to about $3\ \mu\text{m}$ thickness on the opposite facet; (d) near field image (infrared camera) of the TE and TM modes at the output facet of the interposer (shown in (c)); (e) packaged $3\ \mu\text{m}$ thick SOI PIC coupled to a fibre array through an optical interposer.

The coupling loss to optical fibres can be as low as 0.5 dB, provided that the mode field diameter is about 2.5 μm , which is achieved with lensed or tapered fibres or small core fibres with high numerical aperture. When a single PIC requires several input and outputs, fibre arrays must be used instead of single fibres. Given the limited assembly precision of fibre arrays and considering that the tolerance to misalignments scales inversely with the mode size, low loss coupling can be ensured only by arrays of standard single mode fibres (SMFs) with mode size around 10 μm . This requires suitable mode size converters, like the one shown in Figure 2, fabricated by etching arrays of 12 μm wide rib and strip waveguides on a SOI wafer with a 12 μm thick device layer, and then tapering the thickness of the output strip waveguides down to 3 μm by manually polishing each optical interposer chip. Alternatively, light can be coupled to the PIC also vertically from up-reflecting mirrors (URMs, see Figure 1 and Figure 3) relying on total internal reflection (TIR), that are wet etched with a negative angle.

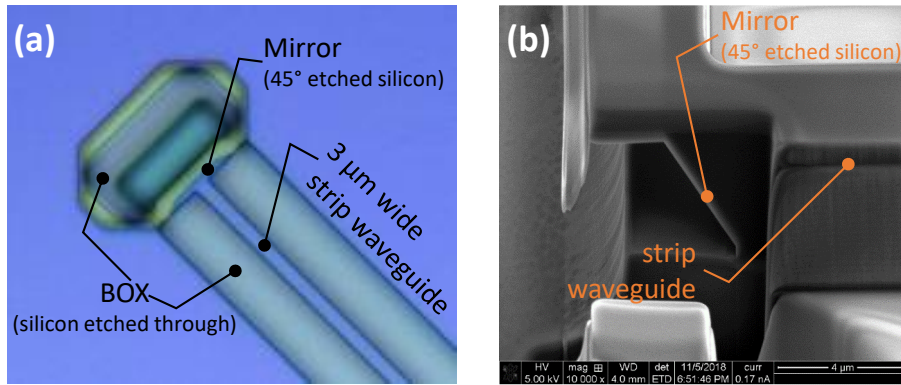


Figure 3. (a) Micrograph of a fabricated URM and (b) lateral cross-section of an URM revealed by focused ion beam.

The anti-reflection coating is the same as for the vertical facets, and coupling losses are practically the same. The wet etching process occurs along crystalline planes, meaning that the mirrors can be fabricated only along the four orthogonal crystal planes with Miller indices 110 , $\bar{1}10$, $1\bar{1}0$, and $\bar{1}\bar{1}0$. One of the advantages of URMs is the possibility to use them to test the fabricated PICs at wafer scale. Compared to grating couplers typically used in submicron waveguides, they support both TE and TM polarisations with negligible polarisation dependent loss, and they operate on the whole transparency range of silicon, from 1.2 μm till 7 μm wavelength. We stress here that thick SOI PICs support operation on the whole transparency range of silicon. In particular, the same rib waveguide can be designed to be singlemode in the whole transparency range, spanning several octaves. At around 3 μm wavelength, absorption in the silica cladding starts affecting the propagation losses that remain below 1 dB/cm till about 4 μm wavelength. Furthermore, low propagation losses can be achieved till 7 μm wavelength by selectively removing the silica cladding¹⁰.

To conclude this section about I/O coupling, we would like to mention that, given the critical impact of losses on quantum devices, we are presently exploring possible further reduction of coupling losses below 0.5 dB by resorting to 3D printed lenses¹¹ and photonic wire bonding¹².

Tight bends enabling high integration density

It is generally assumed that waveguides with micron scale cross-sections require bending radii in the order of several millimetres. This is because the index contrast ensuring singlemode operation in a micron scale waveguide would inherently lead to high radiation losses for tighter bends. In our platform we have developed two solutions to this limitation: turning mirrors based on TIR¹³ (Figure 4(a) and (b)) and tight adiabatic bends⁴ (Figure 4(a)). The first approach applies to both rib waveguides and strip waveguides, whereas the second requires strip waveguides with high index contrast. TIR mirrors allow compact layouts like the imbalanced Mach Zehnder interferometer (MZI) shown in Figure 4(b), also showing the very low-loss (≈ 0.02 dB) waveguide crossings easily achievable on our platform. Turning mirrors can be designed with almost any turning angle, and their losses can be made as low as 0.1 dB per turn by using parabolic shapes and/or making the waveguide sufficiently wide. In fact, the main loss mechanism is light diffraction due to lack of lateral guidance in the mirror region. Remarkably, the turning mirrors work on the whole (1.2 to 7) μm wavelength transparency region of silicon and can be designed to work equally well for both TE and TM polarisation at the same time, despite the polarisation dependent offset induced by the Goos-Hänchen shift¹⁴. Nevertheless, the non-negligible loss makes them unsuitable for circuits requiring a large number of bends like, for example, long spiral waveguides.

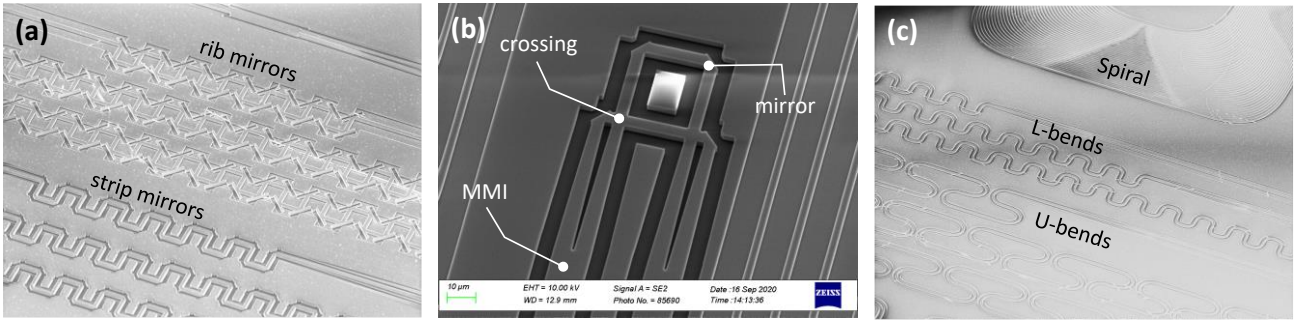


Figure 4. (a) SEM picture of 90° turning mirrors on rib waveguides and strip waveguides; (b) detail of a compact imbalanced MMI based on TIR mirrors; (c) SEM picture of Euler bends with L and U shape and detail of a spiral waveguide using larger L-bends.

For this reason, we have also developed more conventional waveguide bends achieving much lower losses. They are based on strip waveguides, ensuring negligible radiation loss thanks to high light confinement. The only limitation is that they support several HOMs that get easily excited in a tight bend. For this reason, we have introduced⁴ and patented¹⁵ a geometry with gradual change of curvature, resorting to the Euler spiral geometry as shown Figure 4(c) and Figure 5(a) and (b). This way, tight bends with loss lower than 0.02 dB can be achieved with effective bending radii of a few tens of microns, enabling, for example, compact race track resonators with about 4 million Q^5 . Even though, in general, the wavelength range of operation of the bends is not as wide as that of turning mirrors, they can be designed to cover bandwidths of several hundreds of nanometres, up to a few microns.

An interesting property of the Euler bends is that most of supported HOMs (i.e. those with effective index sufficiently higher than the cladding refractive index) are transmitted very efficiently through the bends¹⁶, as highlighted in Figure 5(c). In other words, the bends preserve the mode power distribution, which is useful when designing PICs for mode multiplexing¹⁷ and especially when using spatial modes as a quantum degree of freedom^{18–20} (see also §5). It is also worth mentioning that also turning mirrors preserve the HOM power distribution under reflection²¹.

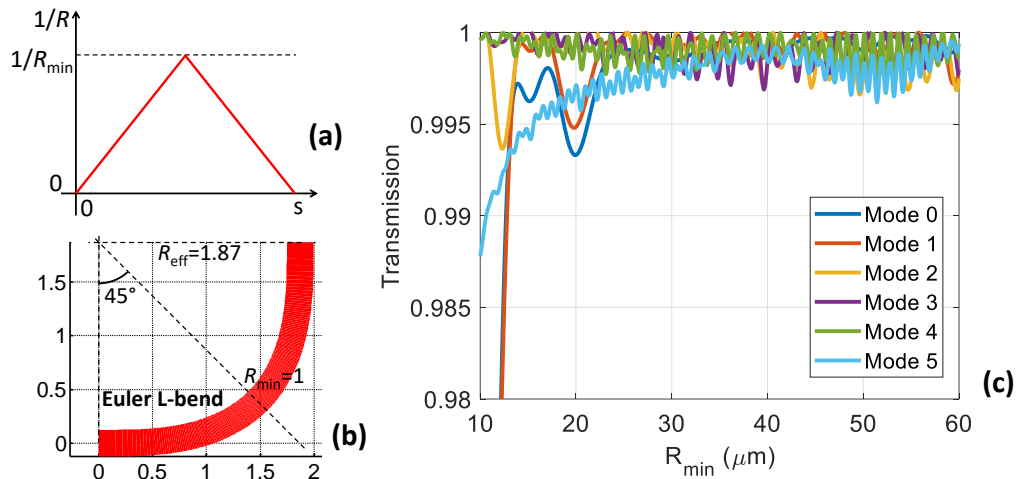


Figure 5. (a) Plot showing the linear change of the curvature $1/R$ as a function of the length s in an Euler bend, starting from zero, reaching up to $1/R_{min}$ and then going back to zero symmetrically; (b) Example layout of a 90° Euler bend (or L-bend) with unitary minimum bending radius, showing the resulting effective radius R_{eff} ; (c) Simulation of the transmission of the fundamental TE_{00} mode and of five horizontal higher order TE modes of a $1.5 \mu\text{m}$ wide strip waveguide at the output a 90° Euler bend as a function of the minimum bending radius. The five HOMs TE_{0n} modes ($n = 1 \dots 5$) have zero nodes in the vertical direction and n nodes in the horizontal direction. The wavelength is $1.55 \mu\text{m}$.

Polarisation management

Micron scale silicon waveguides support both TE and TM polarisation with very similar mode spatial distribution, same propagation losses and very close effective indices. Indeed, strip waveguides with square cross-section support TE and

TM fundamental modes with identical propagation constant, and any possible residual birefringence induced by material strain can be easily compensated by fine tuning the waveguide width. Most of the building blocks, including multimode interference (MMI) splitters, can be designed to support both polarisations at the same time. On the other hand, in many applications (including telecom and sensing) polarisation can be used as a degree of freedom, in which case at least a polarisation splitter/combiner is required and preferably also different types of polarization rotators. We are presently developing a wide portfolio of building blocks for polarisation management, including MZI polarisation beam splitters (PBSs)^{6,22} (see Figure 6(a)) and rotators²³. Remarkably, we have demonstrated the use silicon itself as magneto-optic material and achieved Faraday rotation in zero-birefringence waveguides⁷. Our ultimate goal is to build a fully integrated all-silicon circulator, based on splitters/combiners and reciprocal and non-reciprocal rotators (Figure 6(b)).

We conclude this section mentioning that Faraday mirrors are used in several quantum photonic implementations, including quantum key distribution systems (see §3), to ensure their stable operation^{24,25}. Faraday mirrors can be achieved in the platform by combining a Faraday rotator with a back reflector like a MMI reflector or a Sagnac loop²⁶.

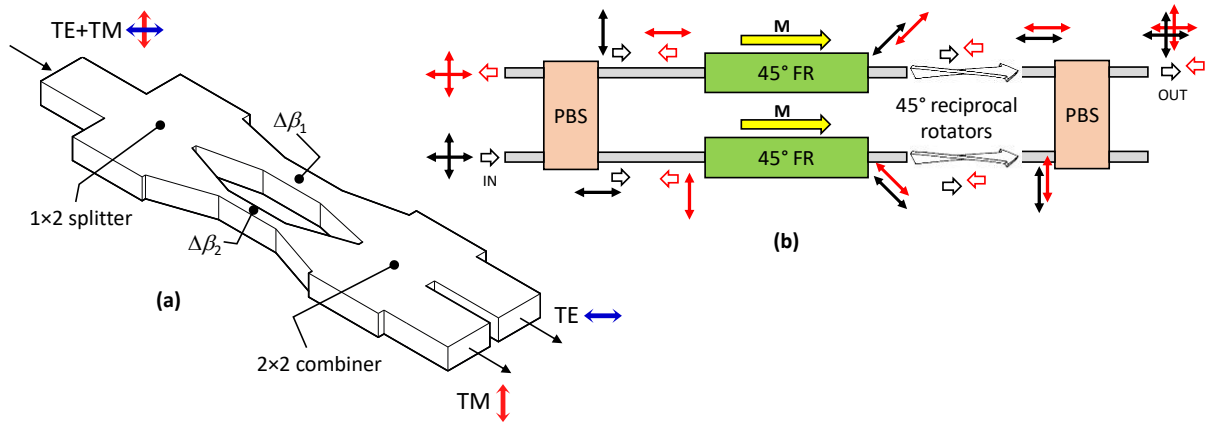


Figure 6. (a) Sketch of a MZI exploiting the form birefringence of waveguides of different width to serve as a PBS; (b) Scheme of a possible implementation of an integrated light circulator by combining PBSs, Faraday rotators (FR) and reciprocal polarization rotators on chip.

Low loss wavelength filters

We have demonstrated several different types of wavelength filters, including multi-million Q ring resonators⁵, compact MMI resonators²⁶, flat-top lattice filters²⁷, and flat-top ring-loaded MZIs²⁸. All these filters can be designed to have less than 0.5 dB excess loss. We have demonstrated also low-loss echelle gratings and arrayed waveguide gratings (AWGs)²⁹. In Figure 7(a) we show the layout of an AWG with small footprint thanks to the use of Euler bends. The device is polarisation independent, thanks to strip waveguides with square cross-section. The excess loss is in the 2 dB to 3 dB range, and the extinction ratio (ER) is larger than 25 dB.

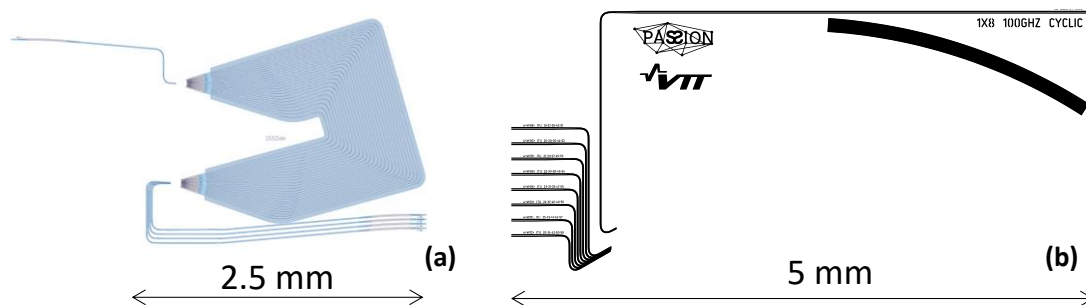


Figure 7. (a) Compact AWG with 100 GHz channel spacing and 5 nm free spectral range exploiting Euler bends and nearly-zero birefringence waveguides, ensuring polarisation independent operation; (b) cyclic echelle grating with 100 GHz channel spacing.

We have also demonstrated AWGs with loss in the 1 dB to 2 dB range²⁹, and ER exceeding 30 dB on all channels. We are presently working on further reduction of the excess loss by improving the design and fabrication of the star coupler. For echelle gratings like the one shown in Figure 7(a) we have already demonstrated excess loss below 1 dB for both polarisations (around 0.8 dB) with extinction ratio exceeding 20 dB for all channels.

Interfacing micro- and nano-scale devices

Recently we have been developing a light escalator³⁰ made of hydrogenated amorphous silicon (a-Si:H) to interface our micron-scale waveguides with submicron waveguides and thin layers including 2D materials and superconducting nanowires. We grow a submicron layer of a-Si:H with refractive index around 3.65 on top of the crystalline device layer, and pattern it to achieve adiabatic transfer of the light from the thick silicon waveguide to the thinner a-Si:H layer with significantly higher refractive index, as can be seen from the simulation in Figure 8(a). The a-Si:H layer thickness can be optimised to maximise the overlap of the propagating light with, e.g., a graphene layer or a superconducting nanowire single photon detector (SNSPD) sandwiched between crystalline silicon (c-Si) and a-Si:H, similar to what sketched in Figure 8(b). Furthermore, crystalline silicon can be also removed selectively away and replaced with a deposited silica layer before depositing the a-Si:H layer, as sketched in Figure 8(c). The resulting high index contrast a-Si:H waveguide allows to interface the microscale waveguide with submicron waveguides including plasmonic slot waveguides or even just PICs based on submicron silicon waveguides that can be simply bonded on top of the a-Si:H waveguide and evanescently coupled via inverse tapers. Both types of escalators can be fabricated using the same fabrication process.

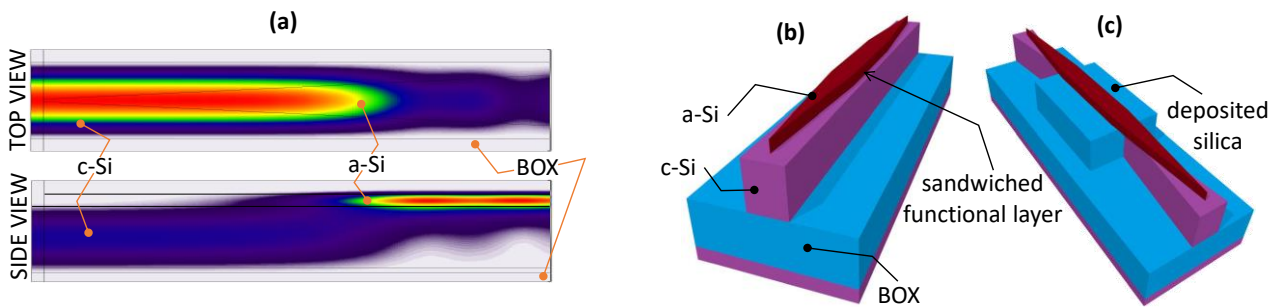


Figure 8. (a) 3D simulation with the eigenmode expansion method of the adiabatic power transfer from a 3 μm thick c-Si waveguide to a 400 nm thick and 200 μm long a-Si:H tapered waveguide fabricated on top; (b) 3D sketch of two escalators to couple light to the a-Si:H waveguide and then back to the 3 μm thick waveguide, showing where a functional layer can be sandwiched between the two silicon types, in the region where the light is guided in a-Si:H; (c) a different type of escalator to couple light to submicron waveguides.

Another unique opportunity to couple our microscale waveguides to nanophotonic devices comes from the URM. In fact, there are cases requiring the light to propagate across a functional surface (unlike the escalator case, where it propagates along it). In these cases, functional surfaces can be fabricated or just transferred on top of the flat output surface of the mirror (which is made of crystalline smooth silicon, not etched). This is a straightforward way to integrate metasurfaces including waveplates³¹, metalenses³², or electro-optic modulators³³.

2.2 Active building blocks

We can divide the actives in two main categories: electrical-to-optical converters (EOCs), which, in our platform, are basically all phase shifters (either thermo-optic or electro-optic), and optical-to-electrical converters (OECs), which are nothing but photodetectors.

Phase shifters

We implement thermo-optic phase shifters by implanting a thin silicon pedestal at the bottom of strip waveguides (Figure 9(a)). We usually cut away the remaining part of the pedestal to achieve higher energy efficiency, reaching about 25 mW per π -shift, with both rise time and decay time of about 15 μs (i.e. speed of about 66 kHz). Very recently, we have also demonstrated about 3 mW per π -shift (still unpublished) by fabricating the heaters on special cavity SOI wafers, which limits the heat flow through the substrate.

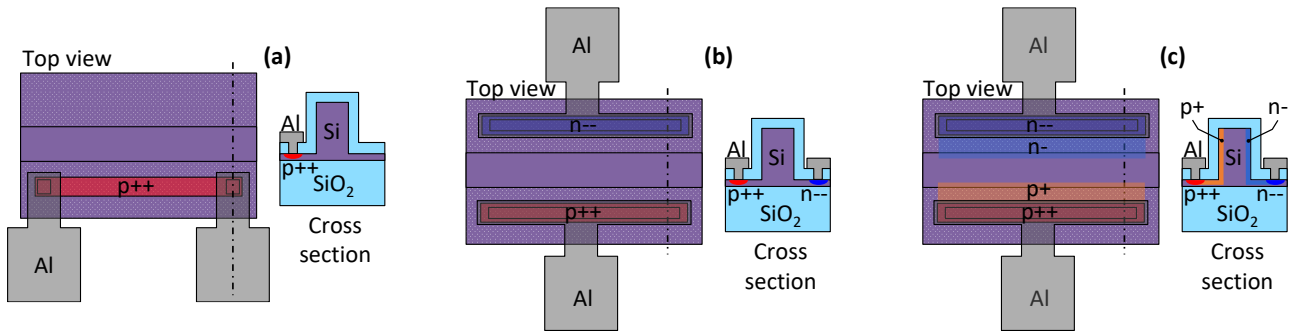


Figure 9. Top views and cross-sections of the three main types of phase shifters available on the platform: (a) thermo-optic (see also Figure 1); (b) electro-optic based on plasma dispersion through carrier injection in a PIN junction; and (c) electro-optic based on EFIPE with a high inverse bias voltage through a PIN junction.

Placing the heaters in direct contact with the silicon layer ensures a significant reduction of the thermal cross-talk³⁴ compared to heaters based on metal wires placed on top of the waveguide upper cladding. This is a major advantage for complex circuits requiring several thermo-optic phase shifters. By design, thermo-optic phase shifters come with no excess loss.

When higher speed is needed, we can reach about 2 to 3 MHz using simple PIN junctions, with only one implantation level, as sketched in Figure 9(b). In this case the refractive index changes thanks to carrier injection inducing plasma dispersion³⁵. The power consumption for a π -shift is lower than 5 mW. Nevertheless, plasma dispersion inherently adds amplitude modulation on top of the phase modulation, due to the Kramers-Kronig relations¹⁴. The loss associated to a π -shift is in the order of 1 dB to 2 dB. Indeed, when made sufficiently long, the same type of PIN junction is also used for variable optical attenuators³⁶.

To overcome these limitations, we are also developing phase modulators relying on the so called electric-field-induced Pockels effect (EFIPE, see Figure 9(c))³⁷, in close collaboration with Prof. Takuo Tanemura's group from the University of Tokyo. For these modulators, we expect significantly lower excess loss thanks to the high reverse bias (electric field of about 40 V/ μm , as close as possible to the breakdown). In particular, we do not expect any major amplitude modulation associated to phase modulation. Furthermore, we aim to reach modulation speeds exceeding 1 GHz, possibly approaching 10 GHz. We also expect the power consumption to be in the microwatt range per π -shift, which is important for cryogenic applications. In fact, EFIPE works well also at cryogenic temperatures³⁸, because it is not affected by carrier freeze-out, unlike plasma dispersion³⁹.

With the goal to achieve extremely low power consumption in combination with modulation speeds exceeding 100 GHz, we are also developing plasmonic modulators in collaboration with Prof. Juerg Leuthold's group from ETH and the company Polariton Technologies⁴⁰. Besides the conventional approach based on nonlinear polymers, we are also exploring the possible use of a-Si:H as nonlinear material based on EFIPE⁴¹. We point out that also plasmonic modulators are particularly suitable for cryogenic applications, since they do not rely on carriers and operate with ultra-low power dissipation⁴². The main limitation of plasmonic phase shifters is the high excess loss, typically exceeding 5 dB.

To conclude this section, we point out that a key missing building block for quantum PICs (QPICs) in all platforms is a suitable phase shifter to ideally ensure at the same time small footprint, ultra-low power consumption, high speed, ultra-low optical loss, and cryogenic operation, or at least a subset of these properties, depending on the application. Recent results demonstrate that microelectromechanical systems (MEMS) are a promising path both for submicron silicon⁴³ and silicon nitride^{44,45} platforms, with losses below 0.5 dB, speeds from a few MHz to beyond 100 MHz, and footprint ranging from about 100 \times 100 μm^2 to 1 \times 1 mm². Instead, in our platform we are presently exploring faster and more compact phase shifters by placing electro-optic metasurfaces³³ on top of URMs, with the goal to access the full nonlinear coefficient of electro-optic polymers, which is typically reduced by one order of magnitude in plasmonic slot waveguides⁴⁶.

Detectors

Our platform includes monolithically integrated germanium (Ge) photodiodes (PD), with responsivity in the order of 1 A/W at 1550 nm wavelength, meaning 80% quantum efficiency. We have developed both high-speed PDs and monitor PDs. The high-speed PDs exceed 40 GHz speed when operated with 1 V reverse bias³, with a dark current of about 4 μA , whereas monitor PDs are operated with lower bias voltage and have about 10 nA dark current with about 1 GHz speed.

We are presently starting the cryogenic characterisation of our PDs to determine the temperature dependence of dark current⁴⁷, responsivity, signal to noise ratio⁴⁸, speed, carrier freeze out, and wavelength range. We are also developing avalanche photodetectors⁴⁹ (APDs) exploiting the avalanche effect in silicon⁵⁰, and also plan to operate them in Geiger mode to achieve single photon avalanche detectors (SPADs)⁵¹.

Besides, in collaboration with Prof. Juerg Leuthold's group from ETH, we are also developing high-speed plasmonic Ge detectors to exceed 100 GHz analog bandwidth⁵². Here the main driver is not the detection efficiency but high-speed operation at a few kelvin, with the goal to develop suitable OECs to transfer a large amount of data to the cryostat. As explained in more details in §4, the idea is to drive superconducting electronics (e.g. single flux quantum, SFQ) using optical fibres.

With cryogenic and quantum applications in mind, we are also developing guided-wave SNSPDs, with the final goal to couple them through the light escalator (Figure 8(b)). In order to speed-up the detector development, we have started fabricating the devices sketched in Figure 10(c). We first oxidised a silicon wafer, deposited superconducting NbN on the thermal oxide, and then patterned the nanowires using e-beam lithography, as shown in Figure 10(a). Next, we have deposited a-Si:H and patterned the waveguides (Figure 10(b)), including inverse tapers to improve fibre coupling from the chip edge. The optical fibre is aligned using a nanopositioner in the cryostat. In parallel, we are also developing amorphous alternatives^{53,54} to crystalline NbN, aiming at improved fabrication yield of the detectors.

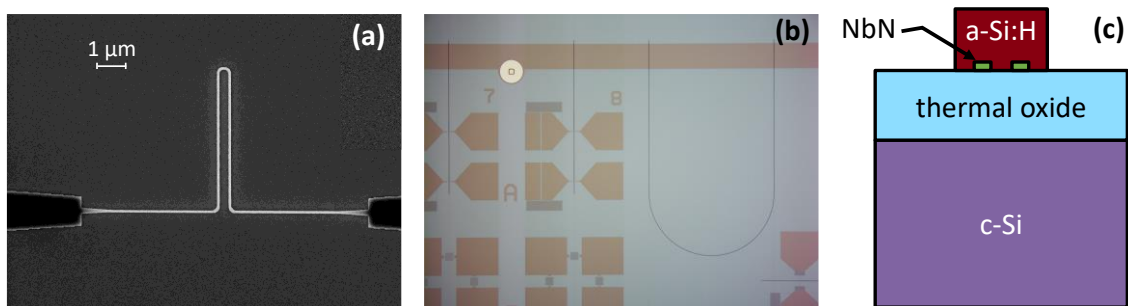


Figure 10. (a) SEM picture of a fabricated NbN SNSPD before a-Si:H deposition; (b) micrograph of a detail of a fabricated chip after etching the a-Si:H waveguides; (c) sketched cross-section of an a-Si:H waveguide with the NbN nanowire embedded.

The SNSPD is the closest thing to an ideal single photon detector demonstrated to date, with detection efficiencies exceeding 97% also in the telecom wavelength range⁵⁵, speeds in the GHz range⁵⁶, jitter even lower than 3 ps⁵⁷ and dark counts even lower than 0.1 Hz⁵⁸. However, for some quantum realisations, and especially those based on Gaussian states, photon number resolution (PNR) is an important capability which is not straightforwardly provided by SNSPDs. A possible solution are transition edge sensors (TESs)⁵⁹, even though they require temperatures in the order of 100 mK that cannot be achieved with closed-cycle table-top cryostats but only with larger dilution refrigerators. Furthermore, their speed is limited to about 1 MHz. Integration of TESs on optical waveguides have been demonstrated already on other platforms^{60,61}, and we could consider integrating them as well, following exactly the same approach we are using for SNSPDs and leveraging the mature free space TES technology we have developed at VTT⁶². On the other hand, in collaboration with Prof. Val Zwiller's group from KTH and with the company Single Quantum, we are also exploring the possible use of single SNSPDs as efficient PNR detectors^{63,64}.

2.3 Hybrid integration

Several different PIC technologies are available, including most mature submicron and micron-scale silicon and silicon nitride¹⁰ platforms, and micron-scale indium phosphide⁶⁵ platforms, as well as the more recent lithium niobate on insulator platforms⁶⁶⁻⁶⁹ and compound on insulator platforms⁷⁰. Each material system comes with its strengths and weaknesses, meaning that suitable combinations of complementary systems are often needed to achieve fully integrated solutions. An exemplary case is the lack of monolithically integrated light sources in all platforms not based on compound semiconductors, where either heterogeneous integration⁷¹ or hybrid integration^{1,72} are needed. Our main focus at VTT is on hybrid integration based on high-precision flip-chip bonding at wafer scale, which is suitable for mid-volume production in a CMOS fab like ours. At variance with heterogeneous and monolithic integration, in the hybrid approach the silicon process and the III-V process (or the process of any other complementary material system) can happen in parallel in two different fabs, which comes with several advantages, including shorter overall lead time, reduced process flow complexity,

reduced constraints and trade-offs for the two material systems, as well as decoupled yield of the two processes, resulting in higher overall yield, i.e. higher cost efficiency. Furthermore, hybrid integration can be made with commercially available dies (e.g. light sources or photodetectors) which can lead to even higher cost efficiency.

By using either vertical facets or URMs, we can easily integrate devices where light propagates respectively in-plane – like distributed Bragg reflector lasers, semiconductor optical amplifiers, or electro-absorption modulators – or out-of-plane – like vertical cavity emitting lasers or free-space photodetectors. In particular, the URM can be a key component for QPICs, being extremely low-loss, broadband and polarisation independent. For example, it can be used to efficiently couple light from deterministic single photon sources based on quantum dots in vertical cavities⁷³ or to couple single photons or gaussian states to arrays of short SNSPDs (see Figure 11b). We stress here that, even though we have a clear path to monolithic integration of SNSPDs (see §2.2), based on the above considerations, hybrid integration will be the most efficient integration approach for large SNSPD arrays till we develop a SNSPD fabrication process with sufficiently high yield.

3. QKD RECEIVERS

A first example application that can be enabled by the thick SOI platform is quantum key distribution (QKD) networks⁷⁴ with higher key rates and/or longer working distance. In fact, PIC solutions are in the roadmap of major QKD players⁷⁵, because of their unmatched stability, and scalability. We have identified a clear path how our platform could support the development and the large-scale deployment of high-performance QKD systems, as briefly presented in the following for both discrete variable (DV) QKD and continuous variable (CV) QKD.

3.1 DV-QKD

DV-QKD systems are the most suitable to cover long distances. The longest QKD link reported to date reached 600 km distance using a special configuration with a central node⁷⁶, whereas the longest point-to-point link exceeded 400 km⁷⁷ (corresponding to about 70 dB loss in ultra-low loss fibres). Best commercial systems are typically limited to the 100 km to 150 km range, mainly to ensure secure communication with key rates high enough to be useful. In fact, in the DV-QKD implementations most suitable for long distances, the key rate scales linearly with the link transmission probability η , which is the probability of a transmitted photon to be detected at the receiver, accounting for all possible transmission and coupling losses as well as the limited detector efficiency. In contrast with classical optical communication links, this key rate scaling implies a large mismatch between the transmission and detection speeds, which is a unique opportunity to combine the fastest optical modulators ever achieved with the most efficient single photon detectors demonstrated to date, namely plasmonic modulators and SNSPDs. Transmitter speeds of present QKD systems are in the order of a few GHz, meaning that plasmonic phase and amplitude modulators could be used to boost the key rate by at least two orders of magnitude, while being still well matched, by SNSPDs on the receiver side. In fact, present commercial SNSPDs can easily exceed 10 MHz count rates with more than 80% detection efficiency and will possibly exceed GHz count rates and 95% detection efficiency in the future. We stress that the high losses of plasmonic modulators, which are a strong limitation for classical optical communication, are not at all a problem for practical DV-QKD transmitters, which are anyway based on strongly attenuated light sources. On the other hand, high losses are not tolerable for the receiver, meaning that plasmonic modulators are not an option for protocols (like the famous BB84) where modulators are needed to choose the measurement basis also on the receiver side. Nevertheless, this is not a strong limitation, given that the most robust protocols for practical DV-QKD rely on passive receivers, requiring no modulators^{77–79}.

The combination of plasmonic modulators and SNSPDs becomes even more attractive when considering that some of the most promising DV-QKD protocols, including measurement device independent (MDI) QKD^{80,81} and twin-field (TF) QKD^{76,82} connect the users through a central unit (completely untrusted) where all the photon detections occur (Figure 11(a)). Large scale deployment of these systems can be achieved by providing all users with low-cost transmitters (achievable with plasmonic chips) while deploying a central detection unit – owned by the operator – to host a table-top closed-cycle cryostat where thousands of SNSPD can be economically cooled down and operated in parallel. In this vision, the cryostat would be connected with tens to hundreds of fibres, and each fibre should carry tens to hundreds of wavelength division multiplexed (WDM) signals. To this goal, we are presently fabricating at VTT low loss AWGs to demultiplex the WDM signals coming from a single fibre and couple them to flip-chip-bonded arrays of SNSPDs designed and fabricated by Single Quantum to match our layout (see Figure 11b). Monolithic integration of AWGs and SNSPDs has been already demonstrated⁸³, but with high losses both for fibre coupling and demultiplexing. Furthermore, monolithic integration of large SNSPD arrays it is still challenging, due to the relatively poor SNSPD fabrication yield. Hybrid integration of SNSPD

chips (with two detectors only) has been recently demonstrated with submicron silicon waveguides⁸⁴ for time multiplexed MDI-QKD. Nevertheless, also in that case, the coupling losses were very high, because grating couplers were used to couple both the optical fibre and the SNSPDs. We are instead aiming at a solution ensuring at the same time high yield, broadband low-loss fibre coupling, and low demultiplexing loss, that can be even made polarization insensitive with a suitable design of the SNSPD geometry⁸⁵. The final goal will be the full monolithic integration of the DV-QKD receiver on our thick-SOI platform, providing much better and stable control of relative phase and time jitter, therefore leading to higher fringe visibility.

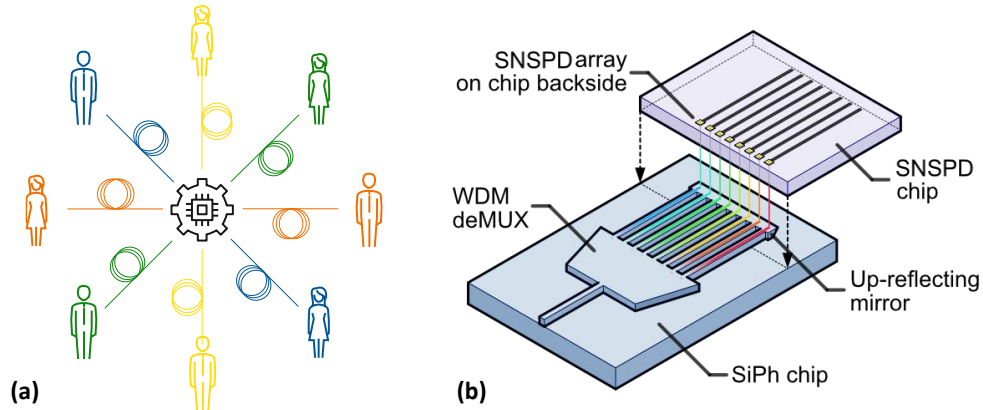


Figure 11. (a) Schematic representation of QKD implementations based on a central node for photon detection, where all the users are equipped with suitable and low-cost transmitters; (b) 3D sketch of the solution we are developing with our partner Single Quantum to address arrays of SNSPDs with low loss and high fabrication yield.

3.2 CV-QKD

An alternative approach is CV-QKD, relying on Gaussian states instead of single photons. The main advantage is that the implementation²⁵ requires only standard telecom components used for classical coherent optical communication and, in particular, there is no need for single photon detectors. The main drawback is that secure implementations scale quadratically with the transmission probability η , which limits the operation range to about 50 km (or to be more rigorous, 10 dB loss, assuming standard 0.2 dB/km fibre loss). Furthermore, unlike DV-QKD, the receiver speed must match the transmitter speed. On the transmitter side, plasmonic modulators are again the perfect choice, given that their losses are not at all an issue, and they can easily achieve both phase and amplitude ultrafast modulation at the same time⁴². Ultrafast phase modulation would be needed also on the receiver side, but luckily on the local oscillator only and not on the quantum states²⁵, meaning that some modulator losses are acceptable. Detection is typically made using shot-noise-limited balanced pulsed homodyne detectors²⁵, which operation speed and stability can greatly benefit from PIC integration and dedicated electronics⁸⁶. We therefore plan to exploit the fast Ge PDs in our platform in combination with our in-house expertise in ultra-fast electronics^{87,88} to develop balanced photodetectors with speed beyond 50 GHz. We stress that, even though the speed of our present Ge PDs is limited to about 40 GHz, suitably designed Ge PDs with smaller volume have been recently demonstrated to reach up to 265 GHz⁸⁹. In our vision, the CV-QKD receiver will be monolithically integrated on our thick SOI platform, to include the ultrafast plasmonic phase modulator and the balanced photodiode. Also in this case, the PIC will ensure much better and stable control of relative phase and time jitter compared to realisations based on optical fibres, therefore leading to improved overall performance of the whole QKD system.

On the transmitter side, integration of the plasmonic devices on our platform would not be strictly necessary, but it could anyway ensure improved operation stability, for example through our integrated Faraday mirrors (see §2.1), not available in any other PIC platform. Similar considerations apply to DV-QKD transmitters. Indeed, many practical implementations of both DV- and CV-QKD rely on Faraday mirrors^{25,77,79}.

4. SCALING-UP SUPERCONDUCTING QUANTUM COMPUTERS

A second example application is the use of optical fibres to transfer data to and from superconducting quantum computers aiming to scale-up the number of qubits and achieve useful universal quantum computing. We are currently in the 'Noisy Intermediate-Scale Quantum' (NISQ) era⁹⁰ – which means that significant applications can be expected already in the

short- and medium-term with a limited number of noisy qubits. However, it is generally agreed that universally useful quantum computers will require about one million qubits⁹¹. To date, most advanced universal quantum computers are based on superconducting qubits and operated at temperatures around 100 mK, in order to minimize thermal noise. Electrical transmission lines are used to carry the electrical signals driving and reading the qubits inside the cryostat. Even though this approach is perfectly fine when dealing with a few hundreds of qubits, it starts becoming challenging for thousands of qubits, and not viable anymore when approaching one million of qubits. In fact, electrical cables come with limited bandwidth, high crosstalk, and high thermal conductivity. For these reasons, at VTT we are pioneering the next generation of communication interfaces for cryogenic qubits, using optical fibres and suitable OECs and EOCs. We are developing this technology in parallel with the development of the Finnish quantum computer, which has recently achieved the first milestone of five qubits⁹², and now targeting fifty qubits by 2024.

Our vision is summarised in Figure 12, where a large amount of data from a supercomputer is serialised by a suitable EOC and sent through an optical fibre to a cryogenic OEC to drive a cryogenic classical co-processor based on single flux quantum (SFQ) logic⁹³. After inputting the data into the quantum processor, the SFQ co-processors uses the calculation output to drive a suitable cryogenic EOC that, through another optical fibre, sends the results to a de-serialising OEC communicating back to the supercomputer. The serialiser and de-serialiser are in general needed because the speed of SFQ logic is typically much higher than the speed of standard complementary metal oxide semiconductor (CMOS) electronics. SFQ is a promising choice thanks to its ultra-low energy dissipation, which is mandatory when working at the ultra-low temperatures required by superconducting quantum computers.

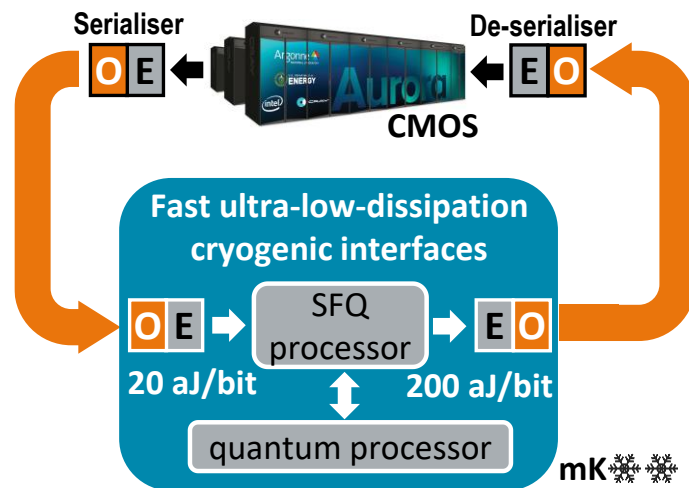


Figure 12. Schematic representation of our plans to use optical fibre links to interface cryogenic quantum computers with supercomputers.

CMOS itself can also be used in cryogenic environments, allowing lower operating voltages and thus lower power consumption^{94,95}, but more dramatic gains in energy efficiency are possible using single flux quantum (SFQ) technology. The latter, and its variants such as energy efficient SFQ, represent bits as short (≈ 1 ps) pulses produced by switching processes in superconducting tunnel junctions called Josephson junctions. The typical energy of these pulses is only 0.2 aJ and they can be processed at speeds exceeding 100 GHz⁹⁶.

As part of this vision, we are presently developing, together with our partners, several PIC solutions for different building blocks. For example, in Figure 13 we show our long-term vision how to replace our prototype serialiser, presently built in our labs based on optical fibres and discrete components, with a fully integrated PIC solution. A III-V reflective semiconductor optical amplifier (RSOA), including a saturable absorber (SA), is flip-chip bonded on the silicon chip where it is coupled to an integrated compact and low-loss external cavity to create an integrated mode-locked laser (IMLL). The generated wavelengths are then separated by a low-loss integrated demultiplexer. The signal in each waveguide is then modulated independently through an array of amplitude modulators, each driven by relatively slow electrical signals (1 GHz to 2.5 GHz). The resulting signals are first delayed by multiples of a suitable delay unit, and finally recombined through a wavelength multiplexer. We are presently fabricating passive PICs combining the delay lines and the final multiplexer, and plan to test it as part of the free-space serialiser prototype already built in our labs.

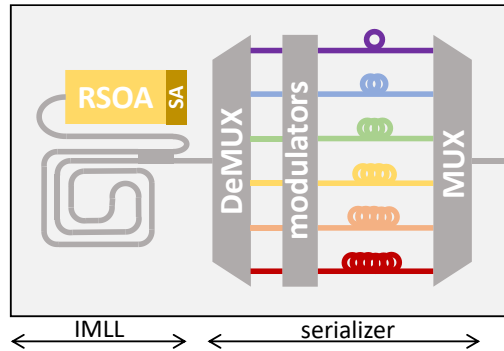


Figure 13. Long term vision of a PIC based serialiser, including an integrated mode-locked laser (IMLL) as multi-wavelength light source.

A second example is the cryogenic OEC that we are building using SNSPD. In this particular application we are more interested in the detection speed rather than extremely high detection efficiency, given that we can use multiple photons per pulse. Together with our collaborators, we are trying to achieve the ultimate SNSPD speed. A simple approach is to make the nanowire as short as possible, but experimental results clearly show that latching⁹⁷⁻⁹⁹ becomes an issue in doing so. Active electrical quenching has been also proposed, but without dramatic improvements¹⁰⁰. In order for the OEC speed to approach the SFQ speed, we are also exploring different multiplexing approaches, addressing arrays of SNSPDs instead of single detectors. This would be somehow equivalent to avoid the optical serialiser at room temperature and replace it with an electrical serialiser inside the cryostat¹⁰¹, resulting in a major underexploitation of the fibre bandwidth. The simplest brute force approach is space division multiplexing (SDM), i.e. coupling each SNSPD with a dedicated fibre. We are indeed developing 2D fibre arrays suitable for cryogenic illumination of detector arrays. A finer approach is to use WDM, exactly the same way as in Figure 11(b), where a single fibre carries several wavelengths. Time division multiplexing (TDM) could be also an option, but it would require active control of a network of relatively fast switches.

The most demanding part of the vision in Figure 12 is by far the cryogenic EOC. In fact, by construction, the energy and the voltages available from the SFQ electronics are very low (attojoules per bit and microvolt respectively), meaning that driving a fast optical modulator inside the cryostat is very challenging. Even though plasmonic modulators have been demonstrated to work with < 1 V and attojoule energy level⁴², driving them with SFQ is still non trivial, and requires some major development, which we are presently tackling.

Together with our partners, we are presently developing in parallel the quantum processors, the SFQ processors, as well as PIC-enabled EOCs and OECs, and we plan to start playing with combinations of these different building blocks in the next few years to demonstrate proofs of concepts of our vision.

5. OTHER INTERESTING APPLICATIONS AND CONCLUSIONS

To conclude, we briefly mention that the thick SOI technology can support many other quantum technology developments. For example, we have just started a project with Prof. Katia Gallo from KTH to integrate their thin lithium niobate waveguides⁶⁹ on our platform. We have also ongoing discussions with Prof. Robert Fickler from Tampere University how to exploit the multimode behaviour and mode preservation capabilities of our PICs (see §2.1) to support spatial shaping of their qudits^{19,20}. We have also identified turbulence mitigation¹⁰² for satellite QKD as a promising application of our low-loss PICs with efficient phase shifters and integrated responsive detectors. We have also ongoing discussions how to support the development of photonic quantum computers, silicon spin qubits, ion traps and diamond nitrogen-vacancy centres.

Eventually, we mention that for all our developments we can constantly rely on our optical labs, where we can characterise PICs electrically and optically both at room temperature and in cryostats, also with the help of our packaging experts.

To summarise, we have introduced our thick SOI platform, with a special focus on the unique features that make it attractive for different quantum technologies, also giving an overview of the ongoing developments that will make it even more attractive in the near future. We have then presented two concrete cases, elaborating in detail our vision how PIC-based solutions will be able to support the large-scale deployment of high-performance QKD networks, based on both DV-QKD and CV-QKD, as well as the scaling-up of useful superconducting quantum computers.

ACKNOWLEDGMENTS

This work has been supported by the European Union's Horizon 2020 Research and Innovation Programme through the project [aCryComm](#), FET Open Grant Agreement no. 899558. We acknowledge also support by the Academy of Finland Flagship Programme, Photonics Research and Innovation ([PREIN](#)), decision number 320168, and by the VTT internal quantum initiative "Quantum leap in quantum control". This work was performed as part of the Academy of Finland Centre of Excellence program (project 336817). We also acknowledge financial support from Business Finland through QuTI-project (grant agreement no. 40562/31/2020).

I thank my colleagues Emma Mykkänen, Tapani Vehmas, Giovanni Delrosso, Katia Kohopää, Markku Kapulainen, Pekka Pursula, Mikko Kiviranta, and Himadri Majumdar as well as our collaborators Val Zwiller, Mario Castañeda, Stephan Steinhauer, Samuel Gyger, Eva De Leo, and Stefan Köppli for their inputs and fruitful discussions.

REFERENCES

- [1] Aalto, T., Cherchi, M., Harjanne, M., Bhat, S., Heimala, P., Sun, F., Kapulainen, M., Hassinen, T. and Vehmas, T., "Open-Access 3- μm SOI Waveguide Platform for Dense Photonic Integrated Circuits," *IEEE J. Sel. Top. Quantum Electron.* **25**(5), 1–9 (2019).
- [2] Bera, A., Marin, Y., Harjanne, M., Cherchi, M. and Aalto, T., "Ultra-low loss waveguide platform in silicon photonics," presented at Silicon Photonics XVII, 24 January 2022, San Francisco, CA, USA, 12006–4, SPIE.
- [3] Vehmas, T., Kapulainen, M., Heimala, P., Delrosso, G., Sun, F., Gao, F. and Aalto, T., "Monolithic integration of up to 40 GHz Ge photodetectors in 3 μm SOI," *Silicon Photonics XV* **11285**, 112850V, International Society for Optics and Photonics (2020).
- [4] Cherchi, M., Ylinen, S., Harjanne, M., Kapulainen, M. and Aalto, T., "Dramatic size reduction of waveguide bends on a micron-scale silicon photonic platform," *Opt. Express* **21**(15), 17814–17823 (2013).
- [5] Zhang, B., Qubaisi, K. A., Cherchi, M., Harjanne, M., Ehrlichman, Y., Khilo, A. N., Khilo, A. N., Khilo, A. N. and Popović, M. A., "Compact multi-million Q resonators and 100 MHz passband filter bank in a thick-SOI photonics platform," *Opt. Lett.* **45**(11), 3005–3008 (2020).
- [6] Shahwar, D., Cherchi, M., Harjanne, M., Kapulainen, M. and Aalto, T., "Polarization splitters for micron-scale silicon photonics," *Silicon Photonics XVI* **11691**, 1169104, SPIE (2021).
- [7] Jalas, D., Hakemi, N., Cherchi, M., Harjanne, M., Petrov, A. and Eich, M., "Faraday rotation in silicon waveguides," 14th Int. Conf. Group IV Photonics, 141–142, IEEE, Berlin, Germany (2017).
- [8] Gao, F., Ylinen, S., Kainlauri, M. and Kapulainen, M., "A Modified Bosch Process For Smooth Sidewall Etching," *Proc. 22nd Micromechanics Microsyst. Technol. Eur. Workshop*, 69–72, Vestfold University College, Toensberg, Norway (2011).
- [9] Gao, F., Ylinen, S., Kainlauri, M. and Kapulainen, M., "Smooth silicon sidewall etching for waveguide structures using a modified Bosch process," *J. MicroNanolithography MEMS MOEMS* **13**(1), 013010–013010 (2014).
- [10] Rahim, A., Goyvaerts, J., Szelag, B., Fedeli, J.-M., Absil, P., Aalto, T., Harjanne, M., Littlejohns, C., Reed, G., Winzer, G., Lischke, S., Zimmermann, L., Knoll, D., Geuzebroek, D., Leinse, A., Geiselman, M., Zervas, M., Jans, H., Stassen, A., et al., "Open-Access Silicon Photonics Platforms in Europe," *IEEE J. Sel. Top. Quantum Electron.* **25**(5), 1–18 (2019).
- [11] Dietrich, P.-I., Blaicher, M., Reuter, I., Billah, M., Hoose, T., Hofmann, A., Caer, C., Dangel, R., Offrein, B., Troppenz, U., Moehrl, M., Freude, W. and Koos, C., "In situ 3D nanoprinting of free-form coupling elements for hybrid photonic integration," *Nat. Photonics* **12**(4), 241–247 (2018).
- [12] Lindenmann, N., Balthasar, G., Hillerkuss, D., Schmogrow, R., Jordan, M., Leuthold, J., Freude, W. and Koos, C., "Photonic wire bonding: a novel concept for chip-scale interconnects," *Opt. Express* **20**(16), 17667–17677 (2012).
- [13] Aalto, T., Harjanne, M., Ylinen, S., Kapulainen, M., Vehmas, T. and Cherchi, M., "Total internal reflection mirrors with ultra-low losses in 3 μm thick SOI waveguides," *Proc SPIE* **9367**, 93670B-93670B – 9 (2015).
- [14] Saleh, B. E. A. and Teich, M. C., [Fundamentals of photonics], Wiley, New York (1991).
- [15] Cherchi, M. and Aalto, T., "Bent optical waveguide," WO2014060648 A1 (2014).
- [16] Jiang, X., Wu, H. and Dai, D., "Low-loss and low-crosstalk multimode waveguide bend on silicon," *Opt. Express* **26**(13), 17680–17689 (2018).
- [17] Li, C., Liu, D. and Dai, D., "Multimode silicon photonics," *Nanophotonics* **8**(2), 227–247 (2019).

- [18] Mohanty, A., Zhang, M., Dutt, A., Ramelow, S., Nussenzeveg, P. and Lipson, M., “Quantum interference between transverse spatial waveguide modes,” *Nat. Commun.* **8**(1), 14010 (2017).
- [19] Brandt, F., Hiekkamäki, M., Bouchard, F., Huber, M. and Fickler, R., “High-dimensional quantum gates using full-field spatial modes of photons,” *Optica* **7**(2), 98–107 (2020).
- [20] Piccardo, M., Ginis, V., Forbes, A., Mahler, S., Friesem, A. A., Davidson, N., Ren, H., Dorrah, A. H., Capasso, F., Dullo, F. T., Ahluwalia, B. S., Ambrosio, A., Gigan, S., Treps, N., Hiekkamäki, M., Fickler, R., Kues, M., Moss, D., Morandotti, R., et al., “Roadmap on multimode light shaping,” *J. Opt.* **24**(1), 013001 (2021).
- [21] Wang, Y., Dai, D. and Dai, D., “Multimode silicon photonic waveguide corner-bend,” *Opt. Express* **28**(7), 9062–9071 (2020).
- [22] Aalto, T., “Devices and Methods for Polarization Splitting,” WO2020089530A1 (2020).
- [23] Harjanne, M., Aalto, T. and Cherchi, M., “Polarization Rotator,” WO2020225479A1 (2020).
- [24] Zbinden, H., Gautier, J. D., Gisin, N., Huttner, B., Müller, A. and Tittel, W., “Interferometry with Faraday mirrors for quantum cryptography,” *Electron. Lett.* **33**(7), 586–588 (1997).
- [25] Jouguet, P., Kunz-Jacques, S., Leverrier, A., Grangier, P. and Diamanti, E., “Experimental demonstration of long-distance continuous-variable quantum key distribution,” *Nat. Photonics* **7**(5), 378–381 (2013).
- [26] Cherchi, M., Ylinen, S., Harjanne, M., Kapulainen, M. and Aalto, T., “MMI resonators based on metal mirrors and MMI mirrors: an experimental comparison,” *Opt. Express* **23**(5), 5982–5993 (2015).
- [27] Cherchi, M., Sun, F., Kapulainen, M., Harjanne, M. and Aalto, T., “Flat-top interleavers based on single MMIs,” *Silicon Photonics XV* **11285**, 112850G, International Society for Optics and Photonics (2020).
- [28] Cherchi, M., Sun, F., Kapulainen, M., Vehmas, T., Harjanne, M. and Aalto, T., “Fabrication tolerant flat-top interleavers,” *Proc SPIE* **10108**, 101080V-101080V – 9 (2017).
- [29] Bhat, S., Harjanne, M., Sun, F., Cherchi, M., Kapulainen, M., Hokkanen, A., Delrosso, G. and Aalto, T., “Low Loss Devices fabricated on the Open Access 3 μm SOI Waveguide Platform at VTT,” presented at ECIO, 2019, Ghent.
- [30] Bera, A., Cherchi, M., Tappura, K., Heimala, P. and Aalto, T., “Amorphous silicon waveguide escalator: monolithic integration of active components on 3- μm SOI platform,” *Silicon Photonics XV* **11285**, 1128507, International Society for Optics and Photonics (2020).
- [31] Jiang, Z. H., Lin, L., Ma, D., Yun, S., Werner, D. H., Liu, Z. and Mayer, T. S., “Broadband and Wide Field-of-view Plasmonic Metasurface-enabled Waveplates,” *Sci. Rep.* **4**(1), 7511 (2014).
- [32] Khorasaninejad, M. and Capasso, F., “Metalenses: Versatile multifunctional photonic components,” *Science* (2017).
- [33] Benea-Chelmus, I.-C., Meretska, M. L., Elder, D. L., Tamagnone, M., Dalton, L. R. and Capasso, F., “Electro-optic spatial light modulator from an engineered organic layer,” *Nat. Commun.* **12**(1), 5928 (2021).
- [34] Sabouri, S., Mendoza Velasco, L. A., Catuneanu, M., Namdari, M. and Jamshidi, K., “Thermo Optical Phase Shifter With Low Thermal Crosstalk for SOI Strip Waveguide,” *IEEE Photonics J.* **13**(2), 1–12 (2021).
- [35] Soref, R. and Bennett, B., “Electrooptical effects in silicon,” *IEEE J. Quantum Electron.* **23**(1), 123–129 (1987).
- [36] Zheng, D. W., Smith, B. T. and Asghari, M., “Improved efficiency Si-photonic attenuator,” *Opt. Express* **16**(21), 16754–16765 (2008).
- [37] Timurdogan, E., Poulton, C. V., Byrd, M. J. and Watts, M. R., “Electric field-induced second-order nonlinear optical effects in silicon waveguides,” *Nat. Photonics* **11**(3), 200–206 (2017).
- [38] Chakraborty, U., Carolan, J., Clark, G., Bunandar, D., Gilbert, G., Notaros, J., Watts, M. R. and Englund, D. R., “Cryogenic operation of silicon photonic modulators based on the DC Kerr effect,” *Optica* **7**(10), 1385 (2020).
- [39] Gehl, M., Long, C., Trotter, D., Starbuck, A., Pomerene, A., Wright, J. B., Melgaard, S., Siirola, J., Lentine, A. L. and DeRose, C., “Operation of high-speed silicon photonic micro-disk modulators at cryogenic temperatures,” *Optica* **4**(3), 374 (2017).
- [40] Burla, M., Hoessbacher, C., Heni, W., Haffner, C., Fedoryshyn, Y., Werner, D., Watanabe, T., Massler, H., Elder, D. L., Dalton, L. R. and Leuthold, J., “500 GHz plasmonic Mach-Zehnder modulator enabling sub-THz microwave photonics,” *APL Photonics* **4**(5), 056106 (2019).
- [41] Cherchi, M., “Electro-Optic Plasmonic Devices,” WO2021099686A1 (2021).
- [42] Heni, W., Fedoryshyn, Y., Baeuerle, B., Josten, A., Hoessbacher, C. B., Messner, A., Haffner, C., Watanabe, T., Salamin, Y., Koch, U., Elder, D. L., Dalton, L. R. and Leuthold, J., “Plasmonic IQ modulators with attojoule per bit electrical energy consumption,” *Nat. Commun.* **10**(1), 1–8 (2019).

- [43] Edinger, P., Takabayashi, A. Y., Errando-Herranz, C., Khan, U., Sattari, H., Verheyen, P., Bogaerts, W., Quack, N. and Gylfason, K. B., “Silicon photonic microelectromechanical phase shifters for scalable programmable photonics,” *Opt. Lett.* **46**(22), 5671–5674 (2021).
- [44] Grottko, T., Hartmann, W., Schuck, C. and Pernice, W. H. P., “Optoelectromechanical phase shifter with low insertion loss and a 13% tuning range,” *Opt. Express* **29**(4), 5525–5537 (2021).
- [45] Dong, M., Clark, G., Leenheer, A. J., Zimmermann, M., Dominguez, D., Menssen, A. J., Heim, D., Gilbert, G., Englund, D. and Eichenfield, M., “High-speed programmable photonic circuits in a cryogenically compatible, visible–near-infrared 200 nm CMOS architecture,” *Nat. Photonics*, 1–7 (2021).
- [46] Xu, H., Elder, D. L., Johnson, L. E., Heni, W., Coene, Y. de, Leo, E. D., Destraz, M., Meier, N., Ghinst, W. V., Hammond, S. R., Clays, K., Leuthold, J., Dalton, L. R. and Robinson, B. H., “Design and synthesis of chromophores with enhanced electro-optic activities in both bulk and plasmonic–organic hybrid devices,” *Mater. Horiz.* (2021).
- [47] Pizzone, A., Srinivasan, S. A., Verheyen, P., Lepage, G., Balakrishnan, S. and Van Campenhout, J., “Analysis of dark current in Ge-on-Si photodiodes at cryogenic temperatures,” 2020 IEEE Photonics Conf. IPC, 1–2 (2020).
- [48] Siontas, S., Li, D., Liu, P., Aujla, S., Zaslavsky, A. and Pacifici, D., “Low-Temperature Operation of High-Efficiency Germanium Quantum Dot Photodetectors in the Visible and Near Infrared,” *Phys. Status Solidi A* **215**(3), 1700453 (2018).
- [49] Zhang, Q., Fu, S., Man, J., Li, Z., Cherchi, M., Heimala, P., Harjanne, M., Fei, S., Hiltunen, M., Aalto, T. and Zeng, L., “Low-loss and polarization-insensitive photonic integrated circuit based on micron-scale SOI platform for high density TDM PONs,” 2017 Opt. Fiber Commun. Conf. Exhib. OFC, 1–3 (2017).
- [50] Martinez, N. J. D., Derose, C. T., Brock, R. W., Starbuck, A. L., Pomerene, A. T., Lentine, A. L., Trotter, D. C. and Davids, P. S., “High performance waveguide-coupled Ge-on-Si linear mode avalanche photodiodes,” *Opt. Express* **24**(17), 19072–19081 (2016).
- [51] Vines, P., Kuzmenko, K., Kirdoda, J., Dumas, D. C. S., Mirza, M. M., Millar, R. W., Paul, D. J. and Buller, G. S., “High performance planar germanium-on-silicon single-photon avalanche diode detectors,” *Nat. Commun.* **10**(1), 1086 (2019).
- [52] Salamin, Y., Ma, P., Baeuerle, B., Emboras, A., Fedoryshyn, Y., Heni, W., Cheng, B., Josten, A. and Leuthold, J., “100 GHz Plasmonic Photodetector,” *ACS Photonics* **5**(8), 3291–3297 (2018).
- [53] Mykkänen, E., Bera, A., Lehtinen, J. S., Ronzani, A., Kohopää, K., Hönlgl-Decrinis, T., Shaikhaidarov, R., de Graaf, S. E., Govenius, J. and Prunnila, M., “Enhancement of Superconductivity by Amorphizing Molybdenum Silicide Films Using a Focused Ion Beam,” *Nanomaterials* **10**(5), 950 (2020).
- [54] Häußler, M., Mikhailov, M. Yu., Wolff, M. A. and Schuck, C., “Amorphous superconducting nanowire single-photon detectors integrated with nanophotonic waveguides,” *APL Photonics* **5**(7), 076106 (2020).
- [55] Chang, J., Los, J. W. N., Tenorio-Pearl, J. O., Noordzij, N., Gourgues, R., Guardiani, A., Zichi, J. R., Pereira, S. F., Urbach, H. P., Zwiller, V., Dorenbos, S. N. and Esmail Zadeh, I., “Detecting telecom single photons with 99.5–2.07±0.5% system detection efficiency and high time resolution,” *APL Photonics* **6**(3), 036114 (2021).
- [56] Beutel, F., Gehring, H., Wolff, M. A., Schuck, C. and Pernice, W., “Detector-integrated on-chip QKD receiver for GHz clock rates,” *Npj Quantum Inf.* **7**(1), 40 (2021).
- [57] Korzh, B., Zhao, Q.-Y., Allmaras, J. P., Frasca, S., Autry, T. M., Bersin, E. A., Beyer, A. D., Briggs, R. M., Bumble, B., Colangelo, M., Crouch, G. M., Dane, A. E., Gerrits, T., Lita, A. E., Marsili, F., Moody, G., Peña, C., Ramirez, E., Rezac, J. D., et al., “Demonstration of sub-3 ps temporal resolution with a superconducting nanowire single-photon detector,” *Nat. Photonics* **14**(4), 250–255 (2020).
- [58] Mueller, A. S., Mueller, A. S., Korzh, B., Korzh, B., Runyan, M., Wollman, E. E., Beyer, A. D., Allmaras, J. P., Allmaras, J. P., Velasco, A. E., Craiciu, I., Bumble, B., Briggs, R. M., Narvaez, L., Peña, C., Peña, C., Spiropulu, M. and Shaw, M. D., “Free-space coupled superconducting nanowire single-photon detector with low dark counts,” *Optica* **8**(12), 1586–1587 (2021).
- [59] You, L., “Superconducting nanowire single-photon detectors for quantum information,” *Nanophotonics* **9**(9), 2673–2692 (2020).
- [60] Höpker, J. P., Gerrits, T., Lita, A., Krapick, S., Herrmann, H., Ricken, R., Quiring, V., Mirin, R., Nam, S. W., Silberhorn, C. and Bartley, T. J., “Integrated transition edge sensors on titanium in-diffused lithium niobate waveguides,” *APL Photonics* **4**(5), 056103 (2019).
- [61] Calkins, B., Mennea, P. L., Lita, A. E., Metcalf, B. J., Kolthammer, W. S., Lamas-Linares, A., Spring, J. B., Humphreys, P. C., Mirin, R. P., Gates, J. C., Smith, P. G. R., Walmsley, I. A., Gerrits, T. and Nam, S. W., “High

- quantum-efficiency photon-number-resolving detector for photonic on-chip information processing,” *Opt. Express* **21**(19), 22657 (2013).
- [62] Akamatsu, H., Vaccaro, D., Gottardi, L., van der Kuur, J., de Vries, C. P., Kiviranta, M., Ravensberg, K., D’Andrea, M., Taralli, E., de Wit, M., Bruijn, M. P., van der Hulst, P., den Hartog, R. H., van Leeuwen, B.-J., van der Linden, A. J., McCalden, A. J., Nagayoshi, K., Nieuwenhuizen, A. C. T., Ridder, M. L., et al., “Demonstration of MHz frequency domain multiplexing readout of 37 transition edge sensors for high-resolution x-ray imaging spectrometers,” *Appl. Phys. Lett.* **119**(18), 182601 (2021).
- [63] Single Quantum., “Application Note: Photon Number Resolving Detectors” (2021).
- [64] Cahall, C., Nicolich, K. L., Islam, N. T., Lafyatis, G. P., Miller, A. J., Gauthier, D. J. and Kim, J., “Multi-photon detection using a conventional superconducting nanowire single-photon detector,” *Optica* **4**(12), 1534–1535 (2017).
- [65] Hoefler, G. E., Zhou, Y., Anagnosti, M., Bhardwaj, A., Abolghasem, P., James, A., Luna, S., Debackere, P., Dentai, A., Vallaitis, T., Liu, P., Missey, M., Corzine, S., Evans, P., Lal, V., Ziari, M., Welch, D., Kish, F., Suelzer, J. S., et al., “Foundry Development of System-On-Chip InP-Based Photonic Integrated Circuits,” *IEEE J. Sel. Top. Quantum Electron.* **25**(5), 1–17 (2019).
- [66] Lin, J., Bo, F., Bo, F., Cheng, Y., Cheng, Y., Cheng, Y., Xu, J. and Xu, J., “Advances in on-chip photonic devices based on lithium niobate on insulator,” *Photonics Res.* **8**(12), 1910–1936 (2020).
- [67] Luke, K., Kharel, P., Reimer, C., He, L., Loncar, M., Loncar, M. and Zhang, M., “Wafer-scale low-loss lithium niobate photonic integrated circuits,” *Opt. Express* **28**(17), 24452–24458 (2020).
- [68] Obrzud, E., Denis, S., Sattari, H., Choong, G., Kundermann, S., Dubochet, O., Despont, M., Lecomte, S., Ghadimi, A. H. and Brasch, V., “Stable and compact RF-to-optical link using lithium niobate on insulator waveguides,” *APL Photonics* **6**(12), 121303 (2021).
- [69] Prencipe, A., Baghban, M. A. and Gallo, K., “Tunable Ultranarrowband Grating Filters in Thin-Film Lithium Niobate,” *ACS Photonics* **8**(10), 2923–2930 (2021).
- [70] Chang, L., Cole, G. D., Moody, G. and Bowers, J. E., “CSOI: Beyond Silicon-on-Insulator Photonics,” *Opt. Photonics News* **33**(1), 24–32 (2022).
- [71] Komljenovic, T., Huang, D., Pintus, P., Tran, M. A., Davenport, M. L. and Bowers, J. E., “Photonic Integrated Circuits Using Heterogeneous Integration on Silicon,” *Proc. IEEE* **106**(12), 2246–2257 (2018).
- [72] Kapulainen, M., Ylinen, S., Aalto, T., Harjanne, M., Solehmainen, K., Ollila, J. and Vilokkinen, V., “Hybrid integration of InP lasers with SOI waveguides using thermocompression bonding,” 2008 5th IEEE Int. Conf. Group IV Photonics, 61–63 (2008).
- [73] Somaschi, N., Giesz, V., Santis, L. D., Loredò, J. C., Almeida, M. P., Hornecker, G., Portalupi, S. L., Grange, T., Antón, C., Demory, J., Gómez, C., Sagnes, I., Lanzillotti-Kimura, N. D., Lemaître, A., Auffeves, A., White, A. G., Lanco, L. and Senellart, P., “Near-optimal single-photon sources in the solid state,” *Nat. Photonics* **10**(5), 340–345 (2016).
- [74] Diamanti, E., Lo, H.-K., Qi, B. and Yuan, Z., “Practical challenges in quantum key distribution,” *Npj Quantum Inf.* **2**, npjq201625 (2016).
- [75] Paraïso, T. K., De Marco, I., Roger, T., Marangon, D. G., Dynes, J. F., Lucamarini, M., Yuan, Z. and Shields, A. J., “A modulator-free quantum key distribution transmitter chip,” *Npj Quantum Inf.* **5**(1), 1–6 (2019).
- [76] Pittaluga, M., Minder, M., Lucamarini, M., Sanzaro, M., Woodward, R. I., Li, M.-J., Yuan, Z. and Shields, A. J., “600-km repeater-like quantum communications with dual-band stabilization,” *Nat. Photonics* **15**(7), 530–535 (2021).
- [77] Boaron, A., Boso, G., Rusca, D., Vulliez, C., Autebert, C., Caloz, M., Perrenoud, M., Gras, G., Bussièrès, F., Li, M.-J., Nolan, D., Martin, A. and Zbinden, H., “Secure Quantum Key Distribution over 421 km of Optical Fiber,” *Phys. Rev. Lett.* **121**(19), 190502 (2018).
- [78] Stucki, D., Brunner, N., Gisin, N., Scarani, V. and Zbinden, H., “Fast and simple one-way quantum key distribution,” *Appl. Phys. Lett.* **87**(19), 194108 (2005).
- [79] Boaron, A., Korzh, B., Houlmann, R., Boso, G., Rusca, D., Gray, S., Li, M.-J., Nolan, D., Martin, A. and Zbinden, H., “Simple 2.5 GHz time-bin quantum key distribution,” *Appl. Phys. Lett.* **112**(17), 171108 (2018).
- [80] Comandar, L. C., Lucamarini, M., Fröhlich, B., Dynes, J. F., Sharpe, A. W., Tam, S. W.-B., Yuan, Z. L., Pentyl, R. V. and Shields, A. J., “Quantum key distribution without detector vulnerabilities using optically seeded lasers,” *Nat. Photonics* **10**(5), 312–315 (2016).
- [81] Yin, H.-L., Chen, T.-Y., Yu, Z.-W., Liu, H., You, L.-X., Zhou, Y.-H., Chen, S.-J., Mao, Y., Huang, M.-Q., Zhang, W.-J., Chen, H., Li, M. J., Nolan, D., Zhou, F., Jiang, X., Wang, Z., Zhang, Q., Wang, X.-B. and Pan, J.-W.,

- “Measurement-Device-Independent Quantum Key Distribution Over a 404 km Optical Fiber,” *Phys. Rev. Lett.* **117**(19), 190501 (2016).
- [82] Lucamarini, M., Yuan, Z. L., Dynes, J. F. and Shields, A. J., “Overcoming the rate–distance limit of quantum key distribution without quantum repeaters,” *Nature* **557**(7705), 400–403 (2018).
- [83] Kahl, O., Ferrari, S., Kovalyuk, V., Vetter, A., Lewes-Malandrakis, G., Nebel, C., Korneev, A., Goltsman, G. and Pernice, W., “Spectrally multiplexed single-photon detection with hybrid superconducting nanophotonic circuits,” *Optica* **4**(5), 557–562 (2017).
- [84] Zheng, X., Zhang, P., Ge, R., Lu, L., He, G., Chen, Q., Qu, F., Zhang, L., Cai, X., Lu, Y., Zhu, S. N., Wu, P. and Ma, X., “Heterogeneously integrated, superconducting silicon-photonics platform for measurement-device-independent quantum key distribution,” *Adv. Photonics* **3**(5), 055002 (2021).
- [85] Chi, X., Zou, K., Gu, C., Zichi, J., Cheng, Y., Hu, N., Lan, X., Chen, S., Lin, Z., Zwiller, V. and Hu, X., “Fractal superconducting nanowire single-photon detectors with reduced polarization sensitivity,” *Opt. Lett.* **43**(20), 5017–5020 (2018).
- [86] Bruynsteen, C., Vanhoecke, M., Bauwelinck, J. and Yin, X., “Integrated balanced homodyne photonic–electronic detector for beyond 20 GHz shot-noise-limited measurements,” *Optica* **8**(9), 1146–1152 (2021).
- [87] Forsten, H., Saijets, J. H., Kantanen, M., Varonen, M., Kaynak, M. and Piironen, P., “Millimeter-Wave Amplifier-Based Noise Sources in SiGe BiCMOS Technology,” *IEEE Trans. Microw. Theory Tech.* **69**(11), 4689–4696 (2021).
- [88] Varonen, M., Shekhipoor, N., Gabritchidze, B., Cleary, K., Forstén, H., Rucker, H. and Kaynak, M., “Cryogenic W-Band SiGe BiCMOS Low-Noise Amplifier,” 2020 IEEE MTT- Int. Microw. Symp. IMS, 185–188 (2020).
- [89] Lischke, S., Peczek, A., Morgan, J. S., Sun, K., Steckler, D., Yamamoto, Y., Korndörfer, F., Mai, C., Marschmeyer, S., Fraschke, M., Krüger, A., Beling, A. and Zimmermann, L., “Ultra-fast germanium photodiode with 3-dB bandwidth of 265 GHz,” *Nat. Photonics* **15**(12), 925–931 (2021).
- [90] Preskill, J., “Quantum Computing in the NISQ era and beyond,” *Quantum* **2**, 79 (2018).
- [91] “A Preview of Bristlecone, Google’s New Quantum Processor,” Google AI Blog.
- [92] “Finland’s first 5-qubit quantum computer is now operational.”, <<https://www.vttresearch.com/en/news-and-ideas/finlands-first-5-qubit-quantum-computer-now-operational>> (3 January 2022).
- [93] Holmes, D. S., Ripple, A. L. and Manheimer, M. A., “Energy-Efficient Superconducting Computing—Power Budgets and Requirements,” *IEEE Trans. Appl. Supercond.* **23**(3), 1701610–1701610 (2013).
- [94] Patra, B., Incandela, R. M., Dijk, J. P. G. van, Homulle, H. A. R., Song, L., Shahmohammadi, M., Staszewski, R. B., Vladimirescu, A., Babaie, M., Sebastiano, F. and Charbon, E., “Cryo-CMOS Circuits and Systems for Quantum Computing Applications,” *IEEE J. Solid-State Circuits* **53**(1), 309–321 (2018).
- [95] Bardin, J. C., Jeffrey, E., Lucero, E., Huang, T., Naaman, O., Barends, R., White, T., Giustina, M., Sank, D., Roushan, P., Arya, K., Chiaro, B., Kelly, J., Chen, J., Burkett, B., Chen, Y., Dunsworth, A., Fowler, A., Foxen, B., et al., “A 28nm Bulk-CMOS 4-to-8GHz μ 2mW Cryogenic Pulse Modulator for Scalable Quantum Computing,” 2019 IEEE Int. Solid-State Circuits Conf. - ISSCC, 456–458 (2019).
- [96] Likharev, K. K. and Semenov, V. K., “RSFQ logic/memory family: a new Josephson-junction technology for sub-terahertz-clock-frequency digital systems,” *Appl. Supercond. IEEE Trans. On* **1**(1), 3–28 (1991).
- [97] Lv, C., Zhang, W., You, L., Hu, P., Wang, H., Li, H., Zhang, C., Huang, J., Wang, Y., Yang, X., Wang, Z. and Xie, X., “Improving maximum count rate of superconducting nanowire single-photon detector with small active area using series attenuator,” *AIP Adv.* **8**(10), 105018 (2018).
- [98] Annunziata, A. J., Quaranta, O., Santavicca, D. F., Casaburi, A., Frunzio, L., Ejrnaes, M., Rooks, M. J., Cristiano, R., Pagano, S., Frydman, A. and Prober, D. E., “Reset dynamics and latching in niobium superconducting nanowire single-photon detectors,” *J. Appl. Phys.* **108**(8), 084507 (2010).
- [99] Münzberg, J., Vetter, A., Beutel, F., Hartmann, W., Ferrari, S., Pernice, W. H. P. and Rockstuhl, C., “Superconducting nanowire single-photon detector implemented in a 2D photonic crystal cavity,” *Optica* **5**(5), 658–665 (2018).
- [100] Ravindran, P., Cheng, R., Tang, H., Bardin, J. C. and Bardin, J. C., “Active quenching of superconducting nanowire single photon detectors,” *Opt. Express* **28**(3), 4099–4114 (2020).
- [101] Miki, S., Miki, S., Miyajima, S., China, F., Yabuno, M. and Terai, H., “Photon detection at 1 ns time intervals using 16-element SNSPD array with SFQ multiplexer,” *Opt. Lett.* **46**(24), 6015–6018 (2021).
- [102] Billault, V., Bourderionnet, J., Mazellier, J. P., Leviandier, L., Feneyrou, P., Maho, A., Sotom, M., Normandin, X., Lonjaret, H. and Brignon, A., “Free space optical communication receiver based on a spatial demultiplexer and a photonic integrated coherent combining circuit,” *Opt. Express* **29**(21), 33134–33143 (2021).